Complete fusion in ^{7}Li + ^{144,152}Sm reactions

P. K. Rath,[1] S. Santra,[2,*] N. L. Singh,[1] B. K. Nayak,[2] K. Mahata,[2] R. Palit,[3] K. Ramachandran,[2] S. K. Pandit,[2] A. Parihari,[1] A. Pal,[2] S. Appannababu,[1] Sushil K. Sharma,[3] D. Patel,[1] and S. Kailas[2]

[1]*Department of Physics, The M. S. University of Baroda, Vadodara 390002, India*

[2]*Nuclear Physics Division, Bhabha Atomic Research Centre, Mumbai 400085, India*

[3]*Department of Nuclear and Atomic Physics, Tata Institute of Fundamental Research, Mumbai 400005, India*

(Received 22 December 2012; revised manuscript received 4 September 2013; published 28 October 2013)

Complete fusion cross sections for ^{7}Li + ^{144,152}Sm reactions have been measured at energies around the Coulomb barrier by offline γ-counting technique. Measured cross sections for the above two reactions are found to be similar at energies well above the Coulomb barrier, however, at sub-barrier energies the cross sections for the ^{7}Li + ^{152}Sm system are much higher compared to the ^{7}Li + ^{144}Sm system, manifesting the effect of target deformation. Cross sections for the present reactions at above-barrier energies are found to be larger than previously measured reactions involving ^{6}Li projectile with the same targets, possibly due to smaller breakup probability of ^{7}Li than ^{6}Li. Coupled-channels calculations show that the experimental fusion cross sections for both the systems are enhanced at subbarrier energies and suppressed at above-barrier energies compared to the respective one-dimensional barrier penetration model predictions. The calculations by different models show that the measured complete fusion cross sections at above-barrier energies are suppressed up to ∼25% compared to the theoretical predictions. It also reveals that a large part of the suppression could be due to inelastic and transfer coupling.

DOI: 10.1103/PhysRevC.88.044617 PACS number(s): 25.70.Jj, 25.70.De, 25.70.Mn

I. INTRODUCTION

Study of fusion reactions involving weakly bound (stable or radioactive) projectiles is a subject of topical interest [1–7]. Different observations exist regarding the enhancement or suppression of the complete fusion (CF) cross section $\sigma_{\rm fus}$ compared to the one-dimensional barrier penetration model (1D-BPM) of fusion, around the Coulomb barrier energies [8–11]. It is reported that, at energies above the Coulomb barrier, the complete fusion cross sections for the reactions involving heavy mass or medium mass targets are suppressed by various degrees compared to the one-dimensional barrier penetration model predictions. However, there is no suppression of the fusion cross section observed for the reactions involving light mass and light medium mass targets, e.g., ^{9}Be + ^{64}Zn [12], ^{6,7}Li + ^{59}Co [13], ^{9}Be + ^{19}F, ^{27}Al, ^{28}Si [14], ^{7}Li + ^{12}C [15].

Fusion cross sections for ^{6}Li + ^{144,152}Sm reactions, that we have measured recently [3,7], are found to be enhanced compared to 1D-BPM results at subbarrier energies, but at above-barrier energies they were suppressed by ∼30%. Systematics of the fusion cross sections for the systems involving loosely bound projectiles [3] with medium and heavy mass targets have shown that the fusion suppression factor on an average increases with the atomic number of the target (Z_T) and decreases with the breakup threshold energy of the projectile ($E_{\rm th}$). With the availability of more and more fusion data involving weakly bound projectiles in the literature, several systematic studies on CF suppression factors have been made to find out the effect of $E_{\rm th}$ and Z_T. Gasques *et al.* [16] and Dasgupta *et al.* [17] have shown that the suppression factor for the reactions involving heavy targets (e.g., ^{208}Pb, ^{209}Bi) with projectiles like ^{6,7}Li, ^{9}Be, ^{10,11}B is highly dependent on projectile breakup (alpha separation) threshold energy. In the systematics made by Parkar *et al.* it is observed that the fusion suppression factors for reactions involving medium mass targets (e.g., ^{144}Sm and ^{124}Sn) are not very different from the ones involving heavy mass targets. Later, CF cross sections have been measured for a reaction involving a slightly lighter mass target, i.e., ^{9}Be + ^{89}Y reaction by Palshetkar *et al.* [4] where the cross sections at above-barrier energies are suppressed by ∼20% which is slightly less than the reactions involving ^{9}Be projectile but heavier targets. Thus it is not very clear whether the CF suppression factor is independent of target charge or not. So, it would be of great interest to carry out a systematic study of the suppression factors for as many reactions involving weakly bound projectiles with different targets having a range of mass or charge. Similarly, the study of the suppression factor dependence on projectile breakup threshold is even more interesting. The alpha-separation energies for the ^{6,7}Li and ^{9}Be nuclei are S_α = 1.48, 2.45, and 1.57 MeV, respectively, and it is shown by Lubian *et al.* [18] that the breakup effects on the fusion for the ^{7}Li-induced reactions are much less important than for ^{6}Li and ^{9}Be. Because we have already measured the CF cross sections for ^{6}Li + ^{144,152}Sm reactions, it would be of further interest to study the fusion reaction involving ^{7}Li as a projectile with the above two targets, i.e., for ^{7}Li + ^{144,152}Sm systems and compare with our earlier measurements to obtain directly the suppression factor dependence on breakup threshold energy. Because ^{7}Li has a higher breakup threshold energy than ^{6}Li, one can expect that the complete fusion (CF) suppression factor for the above reactions would be less compared to ^{6}Li + ^{144,152}Sm systems. Secondly it would be interesting to study the role of target deformation versus projectile breakup and their relative importance by comparing the fusion cross

*ssantra@barc.gov.in

sections involving two isotopes of Sm, i.e., ^{144}Sm and ^{152}Sm, having a different target structure as done in our recent work [7] but with a different projectile (^{6}Li).

In the present work the excitation function measurements have been carried out for the complete fusion of ^{7}Li with ^{144,152}Sm at energies ranging from 0.75 to 1.5 times the Coulomb barrier ($V_B^{\rm lab} \approx 26$ MeV). Coupled-channels calculations have been carried out to understand the measured data and investigate the influence of projectile breakup and target deformation on fusion. The paper is organized in the following order. Details of the measurements and data analysis including the statistical model calculations are described in Sec. II. Fusion calculations by different models and the results using different bare nuclear potentials are discussed in Sec. III. Finally the results are summarized in Sec. IV.

II. MEASUREMENTS AND DATA ANALYSIS

The present measurements have been performed at the 14UD BARC-TIFR Pelletron facility, Mumbai, using the ^{7}Li beam incident on ^{144}Sm (94% enriched) and ^{152}Sm (98% enriched) targets. Targets were prepared by the electro-deposition method on Al backing of thickness 2.2 mg/cm^2. The target thicknesses estimated by the Rutherford backscattering measurement are in the range of 450–680 μg/cm^2. For the fusion measurement, the target was mounted with additional Al backing downstream of the beam. The thickness of the Al backing ($\sim$2.2 mg/cm^2) was sufficient to completely stop all the evaporation residues (ERs) produced during irradiation. Beam energies used were in the range of $E_{\rm lab} = 20$–40 MeV, in steps of 1–2 MeV. Each target was irradiated at a particular beam energy for about 4–8 h depending upon the half-life of the expected ERs and their formation cross sections at that energy. The beam current was in the range of 25–60 nA and the beam flux was calculated by the total charge collected in the Faraday cup, placed behind the target using a precision current integrator device. The reaction products, which were stopped in the target and Al backing, were identified by their characteristic γ rays by offline counting using a HPGe detector coupled to a multichannel analyzer. The ^{152}Eu source was used for the energy calibration as well as for the efficiency measurement.

The excited compound nucleus formed in the fusion of ^{7}Li + ^{144,152}Sm gets de-excited mainly by neutron evaporations. The unstable evaporation residues (ERs) of Tb isotopes decay to Gd isotopes by electron capture. The dominant decay channels in the CF reaction of ^{7}Li + ^{144}Sm were observed to be $2n$, $3n$, and $4n$ evaporation, and those for ^{7}Li + ^{152}Sm were $3n$, $4n$, and $5n$ evaporation channels. The nuclear data, such as half-lives ($T_{1/2}$), γ-ray energies (E_γ), and branching ratios (I_γ) for various decay channels are given in Tables I and II.

The cross sections of different ER channels have been obtained from the observed intensities of the γ lines as listed in Tables I and II with branching ratios corresponding to both ground (g) and metastable (m) states of ERs. The intense γ lines were chosen to evaluate the cross sections. The other γ lines corresponding to the same ERs were also used to cross-check the accepted cross-section values. The excitation function of individual ER channels corresponding to ^{7}Li + ^{144}Sm and ^{7}Li + ^{152}Sm reactions are shown in Figs. 1(a) and 1(b), respectively. The ratios of two dominant ER channels, i.e., σ^{3n}/σ^{2n} in the ^{7}Li + ^{144}Sm reaction and σ^{4n}/σ^{3n} in the ^{7}Li + ^{152}Sm reaction are also shown in Figs. 1(c) and 1(d), respectively.

TABLE I. List of observed evaporation residue channels corresponding to CF in the ^{7}Li + ^{144}Sm reaction, and their decay data.

Reactions	ER	$T_{1/2}$	J^π	E_γ(keV)	I_γ (%)
^{144}Sm(^{7}Li,2n)	^{149}Tb^m	4.16 min	$11/2^-$	796.0	90
	^{149}Tb^g	4.118 h	$1/2^+$	352.2	29.3
				853.4	15.4
^{144}Sm(^{7}Li,3n)	^{148}Tb^m	2.2 min	9^+	394.5	96
				784.5	100
	^{148}Tb^g	60 min	2^-	489.0	19.7
				784.4	84
^{144}Sm(^{7}Li,4n)	^{147}Tb^m	1.83 min	$11/2^-$	1397	78
	^{147}Tb^g	1.64 h	$1/2^+$	694.5	37.3
				1152.5	90.2

Statistical model (SM) calculations are performed using the code PACE [19] to study the relative contributions of different ER channels and estimate the contribution from any missing channel. Although the validity of the PACE predictions for ER cross sections involving tightly bound projectiles are well tested, PACE predictions for the absolute ER cross reactions involving weakly bound projectiles may not be correct because of the presence of the projectile breakup channel leading to a reduction in experimental cross section. However, the branching of individual channels with respect to the complete fusion that are calculated by PACE do not change as the decay of the compound nucleus formed by complete fusion follows the normal statistical model. Thus one can use this information on branching to estimate the cross section of the missing channels and then correct the value of the total experimental ER cross section corresponding to complete fusion.

In the SM calculations, the optical model potentials of Perey and Perey [20] have been used for neutron and proton, while that of Huizenga and Igo [21] for alpha-particle emission. For subbarrier energies the ℓ distributions obtained from coupled-channels calculations are used as input. Potential parameters for the above coupled-channels calculations are chosen to reproduce the fusion cross sections at energies above the Coulomb barrier. Finally, to have a consistent description,

TABLE II. List of observed evaporation residue channels corresponding to CF in the ^{7}Li + ^{152}Sm reaction, and their decay data.

Reactions	ER	$T_{1/2}$	J^π	E_γ(keV)	I_γ (%)
^{152}Sm(^{7}Li,3n)	^{156}Tb^g	5.35 d	3^-	199.2	40.9
				356.4	13.6
				534.3	66.6
^{152}Sm(^{7}Li,4n)	^{155}Tb^g	5.32 d	$3/2^+$	163.3	4.44
				180.1	7.45
				262.3	5.29
^{152}Sm(^{7}Li,5n)	^{154}Tb^g	21.5 h	0^+	557.6	5.4
				704.9	4.8
				722.1	7.7

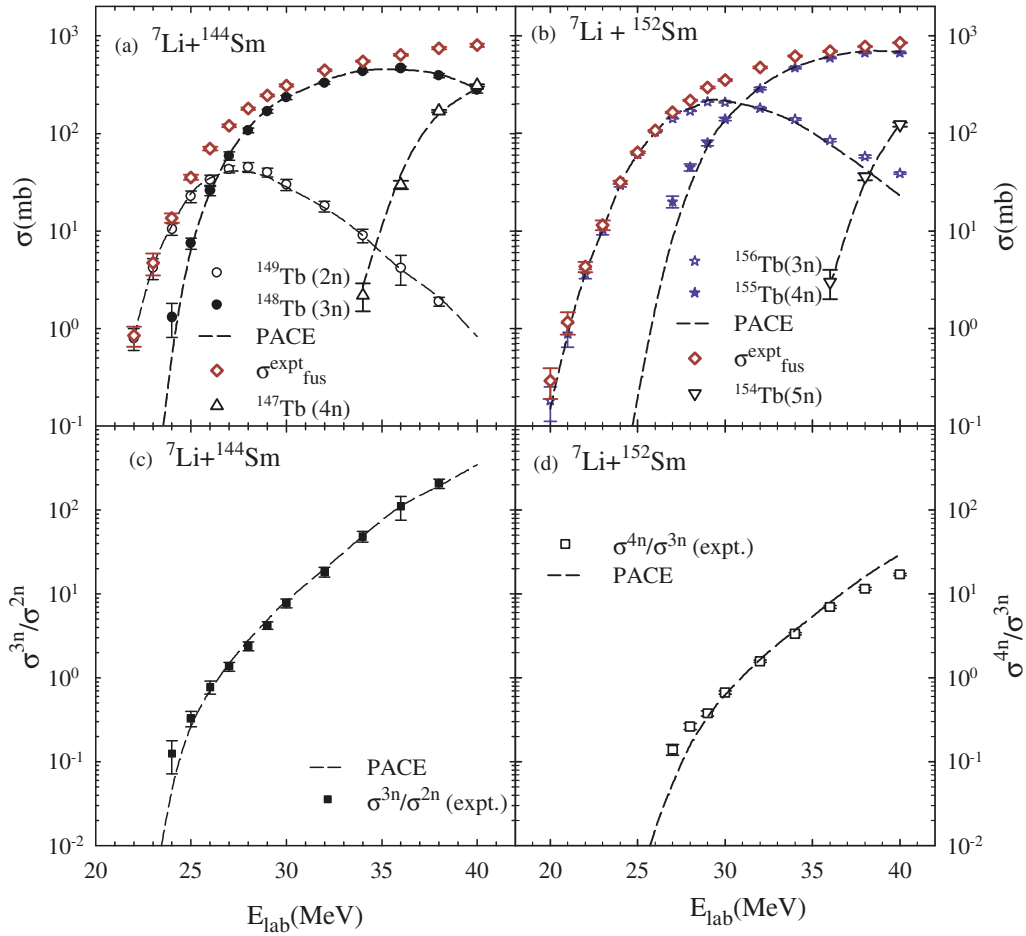

FIG. 1. (Color online) Cross sections for (a) ^{149}Tb ER (hollow circles), ^{148}Tb ER (solid circles), ^{147}Tb ER (hollow triangle-up), and $\sigma_{fus}^{Expt.}$ (hollow diamonds) obtained from the ^{7}Li + ^{144}Sm reaction and (b) ^{156}Tb ER (hollow stars), ^{155}Tb ER (solid stars), ^{154}Tb ER (hollow triangle-down), and $\sigma_{fus}^{Expt.}$ (hollow diamonds) obtained from the ^{7}Li + ^{152}Sm reaction as a function of laboratory energy (E_{lab}). Ratio of two dominant ER channels, i.e., σ_{3n} to σ_{2n} (solid squares) in first reaction and σ_{4n} to σ_{3n} (hollow squares) in second reaction at different beam energies are shown in (c) and (d), respectively. Lines represent the results of statistical model calculations (see text for details).

the SM calculations for all the energies are made using coupled-channels-generated ℓ distribution as an input to PACE. Two important parameters in the statistical model calculations are (i) transmission coefficient of the outgoing particles and (ii) level density of the residual nuclei. The transmission coefficients are calculated by the Hill-Wheeler formula [22]. The level density parameter is "a" $= A/K$ MeV^{-1}, where A is the mass number of the residual nucleus and K is a free parameter. The ER cross sections for xn channels are predicted by SM calculations with three different level density parameters (with "K" = 9, 10, and 11). The calculation with $K = 11$ was found to provide a good description of the present experimental data for ER as well as the ratios over a broad energy range. The results of PACE calculations (dashed lines) for the ratio of σ_{3n} to σ_{2n} for ^{7}Li + ^{144}Sm and σ_{4n} to σ_{3n} for ^{7}Li + ^{152}Sm are shown in Figs. 1(c) and 1(d), respectively.

Using the above parameters in PACE, the branching of the sum of the measured channels (i.e., $\Sigma\sigma_{xn}$ with $x = 2, 3, 4$ for ^{7}Li + ^{144}Sm and $x = 3, 4, 5$ for ^{7}Li + ^{152}Sm) with respect to the complete fusion (σ_{CF}) at each energy have been calculated. The theoretical ratio of combined cross sections of the three channels to the complete fusion R_{σ}^{theory} ($=\frac{\Sigma\sigma_{xn}}{\sigma_{CF}}$) is calculated for both the reactions. The above neutron evaporation channels are found to be dominant for most of the energy range of our measurement. The combined cross sections of xn channels are found to be in the range of 74%–92% of CF for ^{7}Li + ^{144}Sm reaction and 62%–99% of CF for the ^{7}Li + ^{152}Sm reaction. It is observed that except for few energies, the measured cross sections are in the range of ∼85%–99% of the total CF. The remaining contributions ($\sigma^{missing}$) are mostly from the charged particle evaporation channels which are difficult to extract from the measured gamma lines as they are contaminated by the contributions from the transfer/ICF channels. Hence the missing cross sections are estimated from the above calculations and given in Tables III and IV. The experimental complete fusion $\sigma_{fus}^{Expt.}$ is determined by adding the cumulative experimental cross sections of various neutron evaporation channels, i.e., $\Sigma\sigma_{xn}$ to the missing channel cross sections $\sigma^{missing}$. The results are given in Tables III and IV, and also shown (as hollow diamonds) in Figs. 1(a) and 1(b), respectively. The consistency in SM results for different ER channels was checked by using $\sigma_{fus}^{Expt.}$ as an input to PACE.

TABLE III. Measured cross sections for $\Sigma\sigma_{xn}$ $(x = 2, 3, 4)$ evaporation residues and complete fusion along with the R_σ^{theory} and missing cross sections (estimated from PACE) for the $^7\text{Li} + ^{144}\text{Sm}$ reaction.

E_{lab} (MeV)	$\sigma_{2n+3n+4n}^{\text{Expt.}}$ (mb)	R_σ^{theory}	σ^{missing} (mb)	$\sigma_{\text{fus}}^{\text{Expt.}}$ (mb)
22	0.8 ± 0.2	0.92	0.1	0.9 ± 0.2
23	4.2 ± 1.0	0.90	0.5	4.7 ± 1.2
24	11.8 ± 1.2	0.86	1.9	13.7 ± 1.5
25	30.2 ± 1.7	0.85	5.4	35.6 ± 2.1
26	59.4 ± 2.5	0.85	10.9	70.3 ± 3.1
27	102 ± 3.3	0.85	19	121 ± 4.2
28	153 ± 4.0	0.85	27	180 ± 5.0
29	209 ± 4.1	0.85	36	245 ± 5.1
30	264 ± 6.0	0.85	47	311 ± 8.0
32	373 ± 6.0	0.84	73	446 ± 8.0
34	449 ± 5.0	0.82	49	551 ± 7.0
36	502 ± 10	0.78	195	640 ± 15
38	566 ± 10	0.75	184	750 ± 20
40	593 ± 10	0.74	211	804 ± 29

The total error in $\sigma_{\text{fus}}^{\text{Expt.}}$ includes the experimental error in each ER cross section as well as the uncertainty in the SM calculations. The errors attributed to the measured ER cross sections are mainly from the statistical uncertainties but having small contributions from systematic uncertainties. Because the contributions of the charged particle evaporation channels to CF are small, the uncertainties on the estimation of these missing cross sections are negligible. Care was taken to limit the systematic uncertainties that could arise from different sources such as (i) current integrator reading, (ii) target thickness, (iii) detector efficiency, and (iv) estimation

TABLE IV. Measured cross sections for $\Sigma\sigma_{xn}$ $(x = 3, 4, 5)$ evaporation residues and complete fusion along with the R_σ^{theory} and missing cross sections (estimated from PACE) for the $^7\text{Li} + ^{152}\text{Sm}$ reaction.

E_{lab} (MeV)	$\sigma_{3n+4n+5n}^{\text{Expt.}}$ (mb)	R_σ^{theory}	σ^{missing} (mb)	$\sigma_{\text{fus}}^{\text{Expt.}}$ (mb)
20	0.18 ± 0.07	0.62	0.11	0.29 ± 0.1
21	0.88 ± 0.24	0.75	0.29	1.17 ± 0.3
22	3.63 ± 0.44	0.84	0.67	4.30 ± 0.5
23	10.3 ± 1.2	0.90	1.2	11.5 ± 1.3
24	29.4 ± 1.1	0.93	2.1	31.5 ± 1.2
25	61.0 ± 1.4	0.96	2.8	63.8 ± 1.5
26	104 ± 2	0.97	2	107 ± 3
27	161 ± 3	0.98	3	164 ± 4
28	215 ± 4	0.98	3	218 ± 5
29	291 ± 6	0.99	4	295 ± 7
30	349 ± 7	0.99	4	353 ± 8
32	469 ± 9	0.99	6	475 ± 10
34	611 ± 11	0.99	9	620 ± 12
36	684 ± 10	0.98	12	696 ± 11
38	763 ± 10	0.98	15	779 ± 11
40	830 ± 10	0.98	20	850 ± 12

of gamma yield. The current integrator reading was calibrated using standard Keithley current source. The target thicknesses have been cross-checked by two measurements using different ion beams (proton and ^{16}O) for elastic scattering measurements at backward angles. The absolute energy-dependent efficiency of the HPGe detector was measured every 8–10 h during offline gamma counting using standard radioactive sources of ^{152}Eu and ^{133}Ba and found to remain invariant with time during the whole experiment. However, a small uncertainty (∼1%) in the fitting parameters of the efficiency curve was taken into account in the final error of each ER cross section. So, most of the errors on ER cross sections are from the uncertainties on gamma yield extraction and gamma statistics.

Experimental CF excitation functions for the two reactions $^7\text{Li} + ^{144,152}\text{Sm}$ are also plotted in a reduced scale (to remove the dependence on Coulomb barrier and the geometrical size of the interacting nuclei) as shown in Fig. 2. Two different

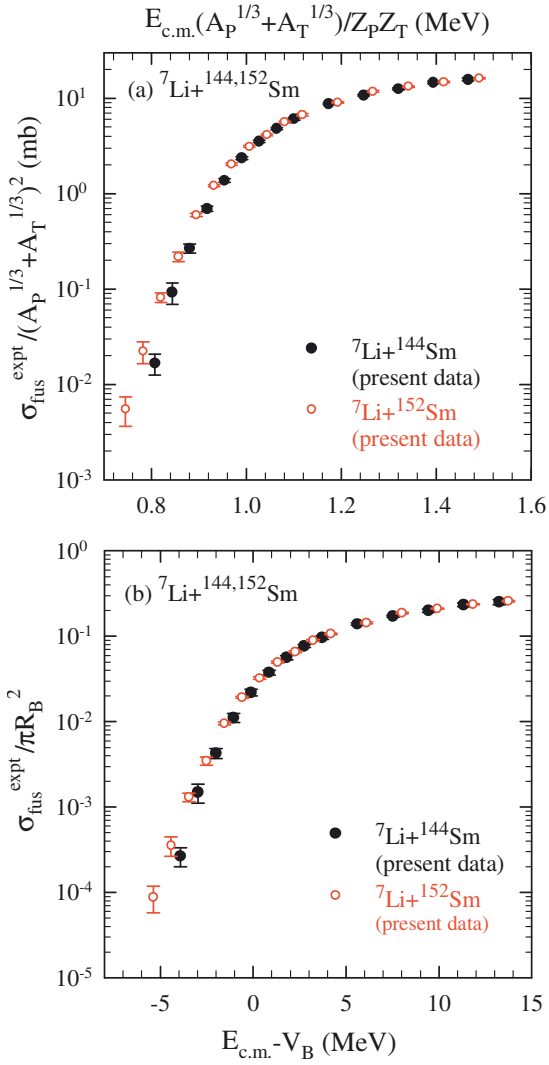

FIG. 2. (Color online) Measured complete fusion cross sections for $^7\text{Li} + ^{144}\text{Sm}$ (solid circles) and $^7\text{Li} + ^{152}\text{Sm}$ (open circles) in reduced scales as a function of reduced energy by two different representations: (a) $\sigma_{\text{fus}}^{\text{Expt.}}/(A_P^{1/3} + A_T^{1/3})^2$ versus $E_{\text{c.m.}}(A_P^{1/3} + A_T^{1/3})/Z_P Z_T$ and (b) $\sigma_{\text{fus}}^{\text{Expt.}}/\pi R_B^2$ versus $E_{\text{c.m.}} - V_B$. See text for details.

reduction procedures have been followed to compare the data in reduced scales. First, in Fig. 2(a) the reduced CF cross section is taken to be "$\sigma_{\rm red} = \sigma_{\rm fus}^{\rm Expt.}/(A_P^{1/3} + A_T^{1/3})^2$" and the reduced energy is taken to be "$E_{\rm red} = E_{\rm c.m.}(A_P^{1/3} + A_T^{1/3})/Z_P Z_T$", where $A_P(A_T)$ and $Z_P(Z_T)$ represent the mass and atomic number of the projectile(target), respectively, as prescribed by Gomes *et al.* [23]. In the second representation, the reduced CF cross section and reduced energies are taken to be "$\sigma_{\rm fus}^{\rm Expt.}/\pi R_B^2$" and "$E_{\rm c.m.} - V_B$," respectively, as shown in Fig. 2(b). Barrier parameters V_B and R_B used for ^{7}Li + ^{144}Sm(^{152}Sm) reaction are equal to 24.9 (24.5) MeV and 10.08 (10.24) fm, respectively. The average fusion barrier V_B is obtained from the experimental fusion barrier distribution (described in the following section). The value of R_B is obtained by adding Coulomb and nuclear potentials. The latter is adjusted to reproduce the experimentally observed average fusion barrier. It can be observed that Figs. 2(a) and 2(b) look similar because of the fact that Coulomb barriers are not very different for the reactions involving same projectile (^{7}Li) and the targets of the same element (Sm). It is observed that at sub-barrier energies the CF cross sections for ^{7}Li + ^{152}Sm (open circles) are higher than those for ^{7}Li + ^{144}Sm (solid circles). The projectile being the same, the enhancement in the CF cross section is certainly from the difference in two targets, i.e., a deformed ^{152}Sm target and a spherical ^{144}Sm target. This observation is similar to the one made in Ref. [7] involving ^{6}Li projectile with the same targets.

Next we have compared the CF cross sections (in a reduced scale) involving two projectiles (^{6,7}Li) with different breakup thresholds but with one particular target, i.e., either ^{144}Sm or ^{152}Sm as shown in Figs. 3(a) and 3(b) respectively. Cross sections for the reactions involving ^{6}Li projectile were taken from the literature [3,7]. To emphasize the difference in cross sections at above-barrier energies, the Y axes are plotted in linear scales. It was observed that the CF cross sections for ^{7}Li-induced reactions at above-barrier energies are larger than those for ^{6}Li for both the targets. It can be concluded that the breakup threshold for ^{6}Li being less than ^{7}Li the loss of incident flux is more for the reactions induced by the former compared to the latter. Thus the CF cross sections for the former are more suppressed from breakup and this observation is consistent with the systematics made by Rath *et al.* [3]. It may be noted that the difference in the above-barrier reduced fusion cross sections between ^{6}Li- and ^{7}Li-induced reactions with deformed ^{152}Sm is not as prominent as in the case of the ^{144}Sm target which may indicate that in addition to projectile breakup other direct reaction channels are also playing some role in the fusion at these energies.

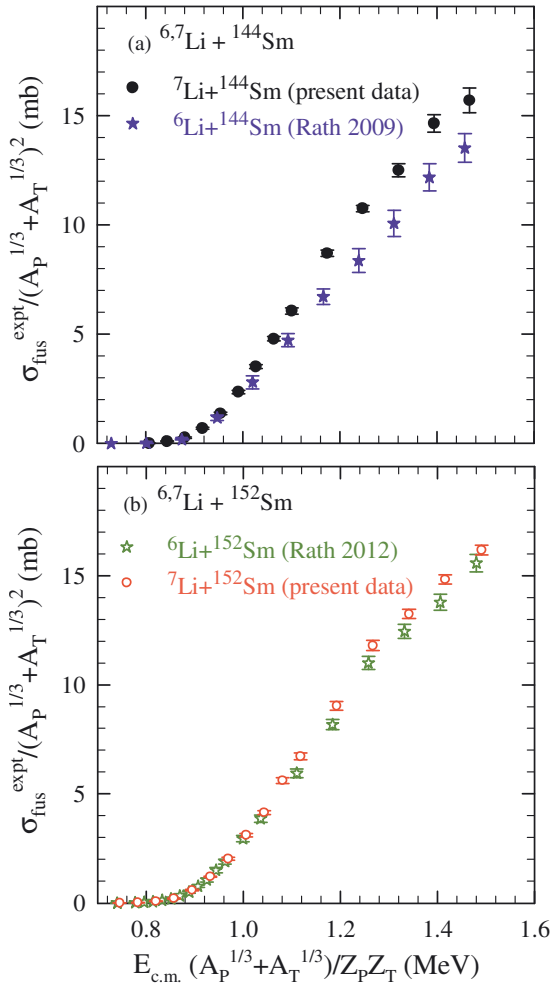

FIG. 3. (Color online) (a) Comparison of CF cross sections involving different projectiles, i.e., ^{6}Li (solid stars) from literature (Rath 2009 [3]) and ^{7}Li (solid circles, present data) but same target (^{144}Sm), showing the effect of projectile breakup threshold. (b) Same as (a) but involving a different target (^{152}Sm) and data for ^{6}Li is from Rath 2012 [7].

III. FUSION CALCULATIONS AND DISCUSSIONS

The fusion cross sections have been calculated using different theoretical models to compare with the measured data and investigate the effect of weak binding of the projectile on fusion if any. For the present work, two different codes based on the coupled-channels (CC) method, CCFULL [24] and FRESCO [25], have been used to calculate the fusion cross section. The simplified CCFULL calculations that can include the couplings to inelastic channels of both projectile as well as target is supposed to provide reasonable descriptions of the fusion cross sections where the effect of transfer couplings is small. Alternately, the FRESCO calculations can include the couplings to both inelastic and transfer channels. One of the most important inputs to the above calculations for fusion cross sections is the appropriate bare nuclear potential for the entrance channel. In the present calculations the parameters for the bare potentials are chosen so as to reproduce the average experimental fusion barrier obtained from the fusion barrier distributions (derived from the present experimental fusion excitation function) as described below.

Fusion barrier distributions have been derived by calculating $d^2(\sigma_{\rm fus}^{\rm Expt.} E_{\rm c.m.})/dE_{\rm c.m.}^2$ using the measured excitation functions for complete fusion ($\sigma_{\rm fus}^{\rm Expt.}$) for the above two reactions. Experimental fusion excitation functions along with barrier distributions for ^{7}Li + ^{144}Sm and ^{7}Li + ^{152}Sm reactions

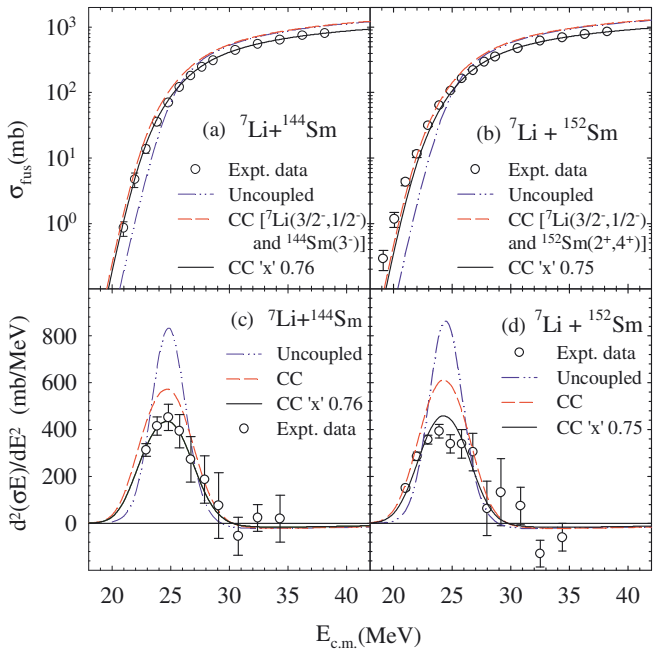

FIG. 4. (Color online) Shown are (a) and (b) the measured complete fusion cross sections (open circles) for $^{7}\mathrm{Li} + ^{144}\mathrm{Sm}$ and $^{7}\mathrm{Li} + ^{152}\mathrm{Sm}$ and (c) and (d) their corresponding barrier distributions. Dash-dot-dot and dashed lines represent the results of coupled-channels calculations for the no-coupling case and with full couplings, respectively. Solid lines are obtained by normalizing the coupled results by 0.76 and 0.75 for $^{7}\mathrm{Li} + ^{144,152}\mathrm{Sm}$ reactions, respectively.

are plotted in Fig. 4 to compare with the coupled-channels calculations described below. The barrier distributions for the two reactions (represented by open circles) are shown in Figs. 4(c) and 4(d). A slight broadening in the width and reduction in the height of the barrier distribution is observed for $^{7}\mathrm{Li} + ^{152}\mathrm{Sm}$ compared to that for $^{7}\mathrm{Li} + ^{144}\mathrm{Sm}$. The average fusion barriers obtained from the experimental barrier distributions are found to be $V_B = 24.9 \pm 0.4$ MeV and 24.5 ± 0.4 MeV for the $^{7}\mathrm{Li} + ^{144,152}\mathrm{Sm}$ systems, respectively. The values of V_B are obtained following the procedure adopted by Dasgupta *et al.* in Ref. [26].

A. CCFULL calculations

Coupled-channels calculations using modified CCFULL code [24], that can include the effect of projectile ground-state spin and the projectile excitation in addition to the target excitation, are performed with the potential parameters that reproduce the average experimental fusion barriers. Potentials used for the coupled-channels (CC) calculations are of Woods-Saxon form with parameters $r_0 = 1.02(1.03)$ fm and $a_0 = 0.63$ fm, and $V_0 = 141(150)$ MeV for $^{7}\mathrm{Li} + ^{144}\mathrm{Sm}$ ($^{152}\mathrm{Sm}$) reaction. The corresponding uncoupled barrier height V_B, radius R_B, and curvature $\hbar\omega$ derived for the present systems are given in Table V.

The full couplings include the coupling of the projectile ground state ($3/2^-$) and first excited state ($1/2^-$, 0.4776 MeV) with β_{00} (β_2 for the ground-state reorientation) = 1.189, β_{01} (β_2 for the transition between the ground and the first excited states) = β_{11} (β_2 for the reorientation of the 1st excited state) = 1.24. The β values are obtained from the ground-state quadrupole moment (-4.06 fm^2 [13,27]) and the BE(2) transition strength (8.3 e^{2}fm^4 [13]) from first excited state to ground state. Regarding target couplings, the vibrational state (3^-, $\beta_3 = 0.23$, $E_x = 1.81$ MeV [28]) was included for ^{144}Sm. The effect of coupling of 2^+ ($\beta_2 = 0.11$, $E_x = 1.66$ MeV) of ^{144}Sm is found to be much less important compared to 3^- state. In the second reaction, because ^{152}Sm is a deformed nucleus in its ground state, both quadrupole (2^+, 0.122 MeV) and hexadecapole (4^+) rotational states with deformation parameters $\beta_2 = 0.26$ and $\beta_4 = 0.05$ [29] are coupled. The coupling to the breakup channel was not included. Results of the coupled-channels calculations with (dashed lines) or without couplings (dashed-dot-dot lines) are shown by different lines in Fig. 4. It was observed that at sub-barrier energies, the calculated fusion cross-sections with only target couplings (not shown in the figure) as well as with target + projectile couplings (dashed lines) are enhanced compared to the uncoupled values. However, at above-barrier energies, the calculated values of CF with or without full couplings are higher than the measured ones. Interestingly, the calculated CF cross sections for $^{7}\mathrm{Li} + ^{144,152}\mathrm{Sm}$ reactions when normalized by 0.76 and 0.75, respectively (solid lines) reproduce the experimental fusion cross-section values at higher energies as well as barrier distribution data very well. Thus, one can conclude that the CF cross sections in this region for the above two reactions are suppressed by $\sim 25 \pm 4\%$ compared to the prediction of CCFULL calculations. The uncertainty of $\pm 4\%$ in suppression factor was estimated from the uncertainties in V_B and $\sigma_{\mathrm{fus}}^{\mathrm{Expt.}}$. Thus the suppression factors for the two reactions are found to be similar but smaller than the ones involving ^{6}Li as a projectile (i.e., $^{6}\mathrm{Li} + ^{144,152}\mathrm{Sm}$ reactions) where the suppression factors are $\sim 32\%$ and 28%, respectively [3,7], when estimated by the same method. These observations are consistent with the systematics made in our earlier work based on projectile breakup threshold and target atomic number [3]. It also shows that the CF at sub-barrier energies is enhanced from both target deformation as well as projectile inelastic state couplings. However, the calculated CF for $^{7}\mathrm{Li} + ^{152}\mathrm{Sm}$ is still underpredicted compared to the experimental data. Similar observation was also made for the $^{6}\mathrm{Li} + ^{152}\mathrm{Sm}$ reaction [7].

TABLE V. Fusion barrier parameters V_B, R_B, and $\hbar\omega$ obtained from potentials used in CCFULL and FRESCO calculations and proximity potential.

Potential	System	V_B (MeV)	R_B (fm)	$\hbar\omega$ (MeV)
Woods-Saxon potential	$^{7}\mathrm{Li} + ^{144}\mathrm{Sm}$	24.9	10.08	4.71
(CCFULL)	$^{7}\mathrm{Li} + ^{152}\mathrm{Sm}$	24.4	10.32	4.61
Sao Paulo potential	$^{7}\mathrm{Li} + ^{144}\mathrm{Sm}$	24.9	10.10	4.20
(FRESCO)	$^{7}\mathrm{Li} + ^{152}\mathrm{Sm}$	24.5	10.30	4.20
Proximity potential	$^{7}\mathrm{Li} + ^{144}\mathrm{Sm}$	24.96	9.95	4.52
	$^{7}\mathrm{Li} + ^{152}\mathrm{Sm}$	24.73	10.06	4.46

The CF suppression factor can also be obtained by a prescription given by Canto *et al.* [30,31] by comparing the universal fusion function (UFF) with the experimental fusion function which are obtained after removing "(i) the static effects of the interacting nuclei, like size and Coulomb barrier, and (ii) the dynamic effects of bound inelastic states and transfer coupling" from the CF cross-section data. Any deviation of experimental fusion function from the UFF should then be because of the dynamic effect of the breakup channels. The fusion cross section and the collision energy are reduced as per the following expressions.

$$E_{\text{c.m.}} \rightarrow x = \frac{E_{\text{c.m.}} - V_B}{\hbar\omega}, \quad F_0(x) = ln[1 + \exp(2\pi x)]. \tag{1}$$

Here x and the universal fusion function $F_0(x)$ are dimensionless variables. The experimental fusion function is then calculated by the following expression,

$$F_{\text{Expt.}}(x) = \left(\frac{2E_{\text{c.m.}}}{\hbar\omega}\sigma_{\text{fus}}^{\text{Expt.}}\right)\frac{\sigma_F^W}{\sigma_F^{\text{CC}}}, \tag{2}$$

where σ_F^W is the fusion cross sections calculated by Wong's formula [32] given by

$$\sigma_F^W = R_B^2\frac{\hbar\omega}{2E}ln\left[1 + \exp\left(\frac{2\pi(E_{\text{c.m.}} - V_B)}{\hbar\omega}\right)\right], \tag{3}$$

and σ_F^{CC} is obtained from the coupled-channels calculations. Following the detailed procedure as given by Canto *et al.* in Refs. [30,31] and using barrier parameters described in Table V, the experimental fusion function $F_{\text{Expt.}}(x)$ and UFF are calculated and compared in Fig. 5. It can be observed that the experimental fusion functions at above-barrier energies are suppressed by about the same factors as obtained from the previous comparison in Fig. 4.

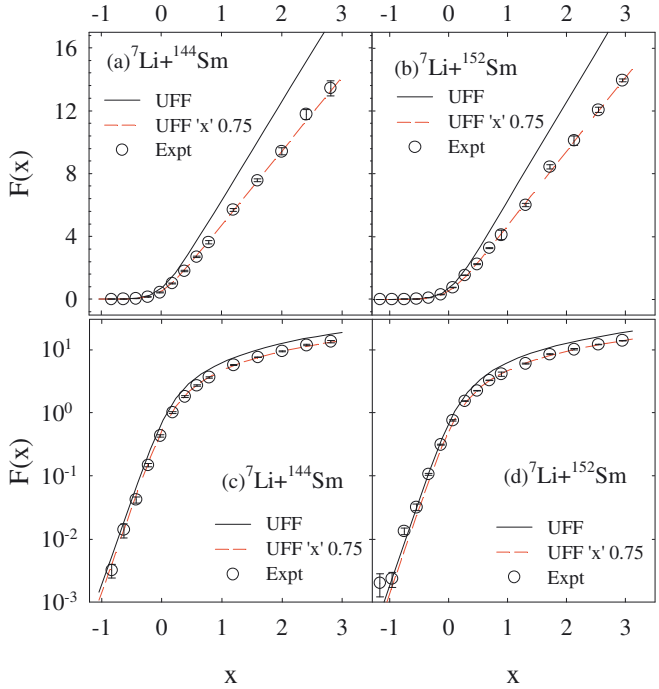

FIG. 5. (Color online) Comparison of universal fusion function (UFF) and experimental fusion function (using the results from CCFULL) as a function of reduced energy "x" in (a) and (b) linear scale and (c) and (d) logarithmic scale (see text for details).

B. FRESCO calculations

To investigate the effect of transfer couplings on fusion cross sections, coupled reaction channel (CRC) calculations are also performed using FRESCO Version 2.9. Here, in addition to the inelastic states of projectile and target as mentioned earlier in CCFULL calculations, transfer channels for $1n$ stripping and $1p$ pickup (with Q value ≈ -1.4 to $+11.0$ MeV) are also included. For $1n$ stripping channels in the reactions ^{144,152}Sm(^{7}Li,^{6}Li)^{145,153}Sm, the ejectile ^{6}Li is assumed to be in the ground state and the residue ^{145}Sm (^{153}Sm) is also taken to be in g.s. or two low-lying excited states. The overlap of ^{7}Li(g.s)/^{6}Li(g.s) has two components: $1p_{1/2}$ and $1p_{3/2}$ with values -0.657 and 0.735, respectively [33]. For $1p$ pickup channels in reactions ^{144,152}Sm(^{7}Li,^{8}Be)^{143,151}Pm, the proton is assumed to have transferred either through the g.s. or first excited state of ^{7}Li with the overlap of ^{7}Li(g.s/0.478 MeV)/^{8}Be(g.s) to be 1.234 and 0.873, respectively [33]. The residue ^{143}Pm (^{151}Pm) is taken to be in g.s. or two low-lying excited states. The details of the transfer channels that are included and their spectroscopic factors are given in Table VI. Inclusion of higher excited states did not show any appreciable change in the fusion cross sections. Other 1-nucleon transfer channels like $1n$ pickup or $1p$ stripping channels are not included as they have large negative Q values (≈ -4.0 to -8.5 MeV) compared to above channels and hence relatively less important.

Because we are interested to see the effect of transfer coupling in addition to the inelastic couplings in the FRESCO calculations, the same set of Woods-Saxon (WS) potential parameters (as used in CCFULL calculations) are used for the entrance channel. For transfer partitions, Sao Paulo (SP)

TABLE VI. Parameters for CRC calculations used in FRESCO.

Reaction	Ejectile/residue States (in MeV)	$J\pi$	Spec. factor	Ref.
^{144}Sm(^{7}Li,^{6}Li)	^{6}Li (g.s)	1^+	0.54 ($1p_{3/2}$)	[33]
^{145}Sm			0.42 ($1p_{1/2}$)	
	^{145}Sm (g.s)	$7/2^-$	0.61	[34]
	^{145}Sm (0.894)	$3/2^-$	0.39	[34]
	^{145}Sm (1.608)	$1/2^-$	0.48	[34]
^{144}Sm(^{7}Li,^{8}Be)	^{8}Be (g.s)	0^+	1.523	[33]
^{143}Pm				[33]
	^{143}Pm (g.s)	$5/2^+$	0.52	[35]
	^{143}Pm (0.272)	$7/2^+$	0.32	[35]
	^{143}Pm (0.960)	$11/2^-$	0.71	[35]
^{152}Sm(^{7}Li,^{6}Li)	^{153}Sm (g.s)	$3/2^+$	1.0	
^{153}Sm	^{153}Sm (0.196)	$13/2^+$	0.71	[36]
	^{153}Sm (0.261)	$3/2^-$	0.97	[36]
^{152}Sm(^{7}Li,^{8}Be)	^{151}Pm (g.s)	$5/2^+$	0.033	[37]
^{151}Pm	^{151}Pm (0.085)	$7/2^+$	0.94	[37]
	^{151}Pm (0.197)	$9/2^+$	0.023	[37]

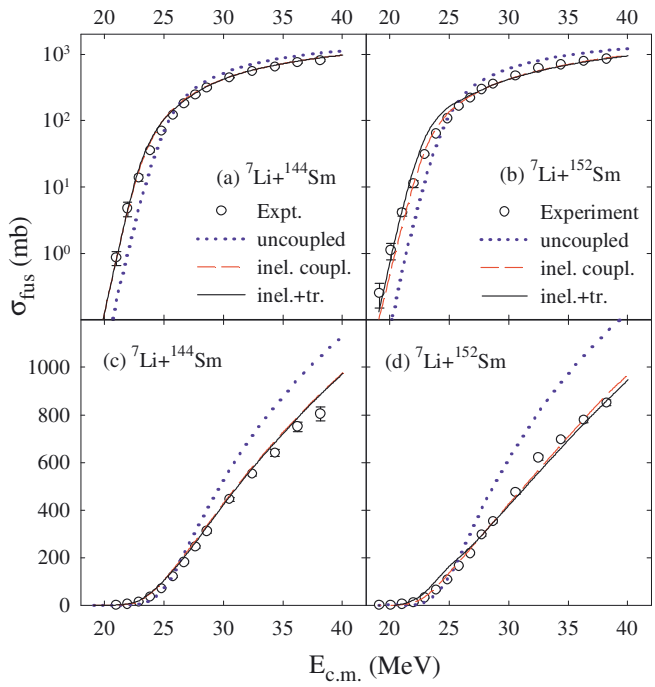

FIG. 6. (Color online) Fusion cross sections calculated by FRESCO using the same WS potential parameters for entrance channel as used in CCFULL with no coupling (dotted line), inelastic coupling (dashed line), and inelastic + transfer coupling (solid line) compared with the experimental data for $^7\mathrm{Li} + ^{144,152}\mathrm{Sm}$ reactions in (a) and (b) logarithmic and (c) and (d) linear scale, respectively.

potentials are used. The same β values as mentioned in CCFULL calculations are used for the inelastic states. No long-range volume imaginary potential is used for the above partitions. Only the short-range surface imaginary potentials with radius parameter $r_0 = 1.0$ fm and diffuseness parameter $a_0 = 0.4$ fm are used to simulate the fusion cross sections to be same as the cumulative absorption cross section. The depth of the imaginary potential is kept at ∼20–30 MeV to have maximum absorption. Fusion cross sections calculated by FRESCO for $^7\mathrm{Li} + ^{144,152}\mathrm{Sm}$ reactions with no coupling, only inelastic coupling, and inelastic + transfer coupling are shown in Fig. 6 by dotted, dashed, and solid line, respectively. The results show that because of coupling of inelastic and transfer channels the fusion cross sections are enhanced at sub-barrier energies and they are suppressed at above-barrier energies. Interestingly, it is observed that the above-barrier cross sections with only inelastic coupling obtained from FRESCO are much closer to the experimental data compared to the ones obtained from CCFULL. Thus it can be concluded that the value of calculated fusion cross sections are model dependent. It is also observed that the effect on fusion by transfer couplings is negligible compared to that by inelastic coupling.

Next we performed the FRESCO calculations using the Sao Paulo potential for the entrance channel to investigate the difference in calculated fusion cross sections from change in the form of the real potential. Here, the SP potentials were normalized by a factor of 0.47 (0.48) to reproduce the average experimental fusion barrier for $^7\mathrm{Li} + ^{144}\mathrm{Sm}(^{152}\mathrm{Sm})$ reaction, although the width of the barrier ($\hbar\omega$) turns out to be slightly different from the ones obtained from the previous set of potential parameters (see Table V). Coupling parameters for the inelastic states and the potentials and spectroscopic amplitudes for the transfer channels remain the same as earlier. From the present FRESCO calculations for the two reactions with inelastic + transfer coupling the fusion cross sections are also found to be very close to the experimental data (not shown in figure). Though, the cross sections at above-barrier energies are found to be slightly larger (specially for $^7\mathrm{Li} + ^{152}\mathrm{Sm}$) than the ones in Fig. 6. Thus, a change in the form of the real potential can also lead to a small difference in the fusion cross section predicted even by the same model.

To find the effect of breakup on CF cross sections, the reduced experimental CF cross sections $F_{\mathrm{Expt.}}(x)$ (symbols) and the UFF (solid line) have been calculated using the above results from FRESCO and the barrier parameters from Table V following the prescription given by Canto *et al.* [30,31]. The results are shown in Fig. 7. The hollow circles (stars) correspond to the $F_{\mathrm{Expt.}}(x)$ which are obtained using the FRESCO results when the Wood-Saxon (Sao Paulo) type of potential was used for the entrance channel. The figure shows that the values of $F_{\mathrm{Expt.}}(x)$ for $^7\mathrm{Li} + ^{144}\mathrm{Sm}$ at sub-barrier energies match with the UFF but at above-barrier energies they are suppressed. Dashed lines in Figs. 7(a) and 7(c) are obtained by multiplying the UFF (solid line) by 0.88. It was observed that the values of $F_{\mathrm{Expt.}}(x)$ for $^7\mathrm{Li} + ^{144}\mathrm{Sm}$ at above-barrier energies are suppressed by about 9%–12% depending upon the kind of potential used for the entrance channel. This

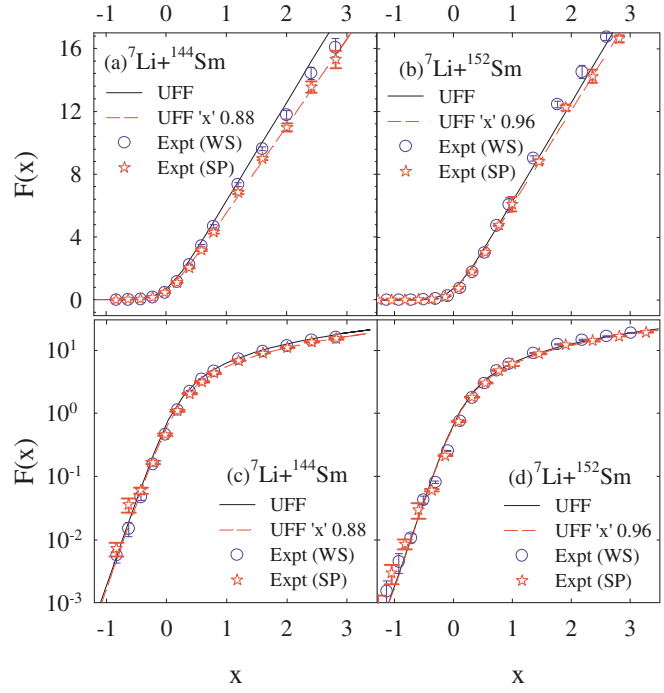

FIG. 7. (Color online) Comparison of UFF (solid line) and experimental fusion function (using the results from FRESCO) as a function of reduced energy "x" in (a) and (b) linear scale and (c) and (d) logarithmic scale. Stars (hollow circles) correspond to the $F_{\mathrm{Expt.}}(x)$ obtained using the fusion from FRESCO when the Sao Paulo (Wood-Saxon) form of potential was used for the entrance channel.

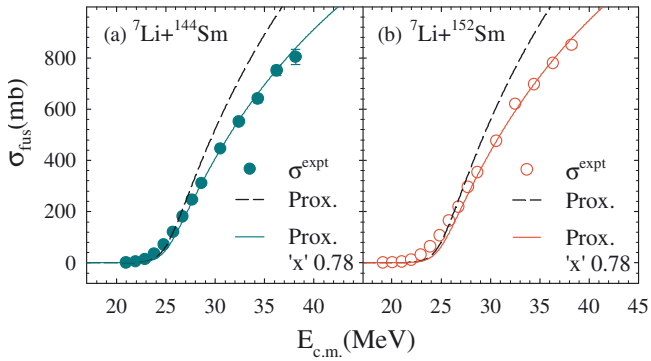

FIG. 8. (Color online) Fusion cross sections calculated for (a) ^{7}Li + ^{144}Sm and (b) ^{7}Li + ^{152}Sm reactions by Wong's model using proximity potentials "Proximity 2000" are represented by dashed lines. The above cross sections multiplied by a factor of 0.78 are represented by solid lines. Solid and hollow circles correspond to the measured CF data for ^{7}Li + ^{144,152}Sm reactions, respectively.

suppression factor is much smaller compared to the one found earlier in Fig. 5 using CCFULL results. Similar results are also obtained for the ^{7}Li + ^{152}Sm reaction as shown in Figs. 7(b) and 7(d), where the suppression is found to be up to 4% only. Thus, the above exercises reveal that the fusion suppression compared to a theoretical prediction depends on the model as well as the form of the potential that one uses for the fusion calculations. It also suggests that the reduction in above-barrier fusion cross sections can have a significant contribution from the coupling of bound inelastic states and transfer channels.

C. Fusion cross sections using proximity potential

The CF cross sections for the present systems have also been estimated using "proximity potential" [38–40] which is parametrized from the existing fusion data in the literature for a large number of reactions involving mostly the tightly bound projectiles. Using the above potential and corresponding expressions for the fusion barrier parameters, i.e, the barrier height "V_B," barrier radius "R_B" and barrier curvature "$\hbar\omega$" are obtained for ^{7}Li + ^{144}Sm and ^{7}Li + ^{152}Sm systems as given in Table V. These parameters are used in the simplified Wong's formula to calculate the fusion cross sections [32].

Fusion cross sections thus obtained are shown in Figs. 8(a) and 8(b) as dashed lines. It can be observed that they overestimate the experimental data at above-barrier energies. To reproduce the experimental data at above-barrier energies, the calculated cross sections for both ^{7}Li + ^{144}Sm as well as ^{7}Li + ^{152}Sm reactions are required to be normalized by a factor of 0.78 and the results are represented by solid lines. This may imply that the experimental CF for both the reactions at above-barrier energies is suppressed by ∼22% compared to the theoretical predictions using the proximity potential. This CF suppression factor obtained here is similar to the one obtained by comparing the experimental data with CCFULL predictions but higher than that from FRESCO prediction.

These observations suggest that although the projectile breakup may be playing an important role in reducing the complete fusion cross section at above-barrier energies, the effect of inelastic and transfer couplings on fusion is also very significant. Moreover, the value of the CF suppression factor depends upon the theoretical model that is used for predicting the CF cross section.

IV. SUMMARY

Complete fusion excitation functions for ^{7}Li + ^{144,152}Sm reactions have been measured at energies near and above the Coulomb barrier. The offline γ-counting technique was used to determine the cross sections of various neutron evaporation channels, which are the most dominating channels of decay of the compound nucleus formed by the complete fusion process in the measured energy range. Comparison of two reactions show that CF cross sections for ^{7}Li + ^{152}Sm at sub-barrier energies are enhanced compared to ^{7}Li + ^{144}Sm but they are of similar values at above-barrier energies. Because the projectile is the same for the present reactions, this difference (enhancement) in cross sections at sub-barrier energies for the ^{7}Li + ^{152}Sm reaction is a manifestation of the effect of target (^{152}Sm) deformation. CF cross sections for the present reactions at above-barrier energies are found to be slightly higher compared to the reactions with the same targets but involving ^{6}Li as the projectile [3,7], which is possibly from the difference in the projectile breakup threshold.

Coupled-channel calculations have been performed by CCFULL and FRESCO codes using the bare potentials that reproduce the average fusion barrier derived from the measured fusion excitation functions. Results for both the reactions show an enhancement in fusion at energies below the Coulomb barrier and suppression above the barrier compared to the predictions by the single-barrier penetration model. Couplings to the target and the projectile excited states enhance the fusion cross sections at sub-barrier energies and they get closer to the experimental data for both the models. However, the effect of coupling on fusion at energies above the barrier is found to be different by the two models. In case of CCFULL calculation the effect is negligible but it is significant in case of FRESCO where the calculated cross sections become closer to the data. The CF suppression factors at above-barrier energies have been derived by comparing the measured fusion data with the above calculations and found to vary from 4% to 25% depending upon the coupled-channel model and form of the bare potential used. Therefore, it can be concluded that the CF suppression factor obtained from the present coupled-channel calculations is model dependent.

Fusion cross sections were also calculated by the Wong model using the fusion barrier parameters obtained from the parametrized proximity potentials. A comparison with the measured CF data shows that the predictions at above-barrier energies are much higher which are consistent with the coupled-channel calculations made by CCFULLL.

From the above comparisons it was found that the experimental CF data for ^{7}Li + ^{144,152}Sm reactions at above-barrier energies are definitely suppressed (by ∼20%–25%) compared to the one-dimensional barrier penetration model predictions. However, a significant part of this suppression seems to be contributed by the effect of coupling of the bound inelastic states and transfer channels on fusion and the remaining could be from projectile breakup.

ACKNOWLEDGMENTS

The authors would like to thank the Pelletron crew for the smooth operation of the accelerator during the experiments. One of the authors (P.K.R.) acknowledges the financial support of CSIR (Grant No. 09/114/0178/2011/EMR-I) in carrying out these investigations.

[1] L. F. Canto, P. R. S. Gomes, R. Donangelo, and M. S. Hussein, Phys. Rep. **424**, 1 (2006).
[2] N. Keeley, R. Raabe, N. Alamanos, and J. L. Sida, Prog, Part. Nucl. Phys. **59**, 579 (2007).
[3] P. K. Rath, S. Santra, N. L. Singh, R. Tripathi, V. V. Parkar, B. K. Nayak, K. Mahata, R. Palit, S. Kumar, S. Mukherjee *et al.*, Phys. Rev. C **79**, 051601(R) (2009).
[4] C. S. Palshetkar, S. Santra, A. Chatterjee, K. Ramachandran, S. Thakur, S. K. Pandit, K. Mahata, A. Shrivastava, V. V. Parkar, and V. Nanal, Phys. Rev. C **82**, 044608 (2010).
[5] V. V. Parkar, R. Palit, S. K. Sharma, B. S. Naidu, S. Santra, P. K. Joshi, P. K. Rath, K. Mahata, K. Ramachandran, T. Trivedi *et al.*, Phys. Rev. C **82**, 054601 (2010).
[6] S. Santra, S. Kailas, K. Ramachandran, V. V. Parkar, V. Jha, B. J. Roy, and P. Shukla, Phys. Rev. C **83**, 034616 (2011).
[7] P. K. Rath, S. Santra, N. L. Singh, K. Mahata, R. Palit, B. K. Nayak, K. Ramachandran, V. V. Parkar, R. Tripathi, S. K. Pandit *et al.*, Nucl. Phys. A **874**, 14 (2012).
[8] C. H. Dasso, S. Landowne, and A. Winther, Nucl. Phys. A **405**, 381 (1983).
[9] M. Dasgupta, D. J. Hinde, N. Rowley, and A. M. Stefanini, Annu. Rev. Nucl. Part. Sci. **48**, 401 (1998).
[10] M. S. Hussein, M. P. Pato, L. F. Canto, and R. Donangelo, Phys. Rev. C **46**, 377 (1992).
[11] N. Takigawa, M. Kuratani, and H. Sagawa, Phys. Rev. C **47**, R2470 (1993).
[12] S. B. Moraes, P. R. S. Gomes, J. Lubian, J. J. S. Alves, R. M. Anjos, M. M. Sant'Anna, I. Padrón, C. Muri, R. Liguori Neto, and N. Added, Phys. Rev. C **61**, 064608 (2000).
[13] C. Beck, F. A. Souza, N. Rowley, S. J. Sanders, N. Aissaoui, E. E. Alonso, P. Bednarczyk, N. Carlin, S. Courtin, A. Diaz-Torres *et al.*, Phys. Rev. C **67**, 054602 (2003).
[14] R. M. Anjos, C. Muri, J. Lubian, P. R. S. Gomes, I. Padron, J. J. S. Alves, G. V. Marti, J. O. F. Niello, A. J. Pacheco, O. A. Capurro *et al.*, Phys. Lett. B **534**, 45 (2002).
[15] A. Mukherjee, M. Dasgupta, D. J. Hinde, H. Timmers, R. D. Butt, and P. R. S. Gomes, Phys. Lett. B **526**, 295 (2002).
[16] L. R. Gasques, D. J. Hinde, M. Dasgupta, A. Mukherjee, and R. G. Thomas, Phys. Rev. C **79**, 034605 (2009).
[17] M. Dasgupta, L. R. Gasques, D. H. Luong, R. du Rietz, R. Rafiei, D. J. Hinde, C. J. Lin, M. Evers, and A. Diaz-Torres, Nucl. Phys. A **834**, 147c (2010).
[18] J. Lubian, I. Padron, P. R. S. Gomes, A. M. M. Maciel, R. M. Anjos, S. B. Moraes, J. J. S. Alves, C. Muri, R. Liguori Neto, and N. Added, Phys. Rev. C **64**, 027601 (2001).
[19] A. Gavron, Phys. Rev. C **21**, 230 (1980).
[20] C. M. Perey and F. G. Perey, At. Data Nucl. Data Tables **17**, 1 (1976).
[21] J. R. Huizenga and G. Igo, Nucl. Phys. **29**, 462 (1962).
[22] D. L. Hill and J. A. Wheeler, Phys. Rev. **89**, 1102 (1953).
[23] P. R. S. Gomes, J. Lubian, I. Padron, and R. M. Anjos, Phys. Rev. C **71**, 017601 (2005).
[24] K. Hagino, N. Rowley, and A. T. Kruppa, Comput. Phys. Commun. **123**, 143 (1999).
[25] I. J. Thompson, Comput. Phys. Rep. **7**, 167 (1988).
[26] M. Dasgupta, P. R. S. Gomes, D. J. Hinde, S. B. Moraes, R. M. Anjos, A. C. Berriman, R. D. Butt, N. Carlin, J. Lubian, C. R. Morton *et al.*, Phys. Rev. C **70**, 024606 (2004).
[27] J. Cederberg, D. Olson, J. Larson, G. Rakness, K. Jarausch, J. Schmidt, B. Borovsky, P. Larson, and B. Nelson, Phys. Rev. A **57**, 2539 (1998).
[28] K. Hagino, N. Takigawa, and S. Kuyucak, Phys. Rev. Lett. **79**, 2943 (1997).
[29] U. Gotz, H. Pauli, K. Alder, and K. Junker, Nucl. Phys. **192**, 1 (1997).
[30] L. F. Canto, P. R. S. Gomes, J. Lubian, L. C. Chamon, and E. Crema, J. Phys. G **36**, 015109 (2009).
[31] L. F. Canto, P. R. S. Gomes, J. Lubian, L. C. Chamon, and E. Crema, Nucl. Phys. A **821**, 51 (2009).
[32] C. Y. Wong, Phys. Rev. Lett. **31**, 766 (1973).
[33] A. A. Rudchik, A. T. Rudchik, G. M. Kozeratska, O. A. Ponkratenko, E. I. Koshchy, A. Budzanowski, B. Czech, S. Kliczewski, R. Siudak, I. Skwirczynska *et al.*, Phys. Rev. C **72**, 034608 (2005).
[34] P. R. Christensen, B. Herskind, R. R. Borchers, and L. Westgaard, Nucl. Phys. A **102**, 481 (1967).
[35] B. H. Wildenthal, E. Newman, and R. L. Auble, Phys. Rev. C **3**, 1199 (1970).
[36] J. R. Lien, G. Lovhoiden, J. Rekstad, A. Henriques, C. Gaarde, J. S. Larsen, and S. Y. V. D. Werf, Nucl. Phys. A **412**, 92 (1984).
[37] D. G. Burke and J. C. Waddington, Nucl. Phys. A **193**, 271 (1972).
[38] J. Blocki, J. Randrup, W. J. Swiatecki, and C. F. Tsang, Ann. Phys. (NY) **105**, 427 (1977).
[39] W. Reisdorf, J. Phys. G: Nucl. Part. Phys. **20**, 1297 (1994).
[40] I. Dutt and R. K. Puri, Phys. Rev. C **81**, 064608 (2010).